DØ note # 3141
July 6, 1997

Search for Supersymmetry in Models with Gauge Mediated Supersymmetry Breaking

Sailesh Chopra, Jianming Qian

Department of Physics, The University of Michigan
Ann Arbor, Michigan 48109

ABSTRACT

We search for inclusive high E_T diphoton events with large missing transverse energy in $p\bar{p}$ collisions at $\sqrt{s}$=1.8 TeV. Such events are expected from pair production of charginos and neutralinos within the framework of the minimal supersymmetric standard model with a light gravitino. No excess of events is observed. A 95% CL exclusion region in the supersymmetry parameter space is presented. Lower mass bounds of 150 GeV/c^2 for the lightest chargino and 75 GeV/c^2 for the lightest neutralino are derived. These limits exclude the region of the parameter space suggested for the chargino interpretation of a recent CDF event in the model. The lower mass limit on the lightest neutralino also rules out a large part of the space suggested for the scalar electron interpretation of the event in the model.

1 Introduction

Supersymmetry is a space-time symmetry which predicts that elementary particles come in Boson-Fermion pairs. The absence of these same mass pairs implies that the supersymmetry must be broken. Most of the supersymmetric phenomenological models assumes the supersymmetry is broken in a hidden sector at a scale Λ which is then transmitted to the visible sector of standard model particles and their supersymmetric partners through either gravitational interactions (supergravity-inspired models) or standard model gauge interactions (gauge-mediated models). The supersymmetric models with gauge-mediated supersymmetry breaking have generated considerable theoretical interests recently [1, 2, 3]. In these models, the scale of supersymmetry breaking can be as low as $\Lambda \sim 100$ TeV. Since the gravitino ($\tilde{G}$) mass is directly related to Λ through

$$m_{\tilde{G}} \sim 4.2 \times 10^{-5} \left(\frac{\Lambda}{500 \text{ GeV}}\right)^2 \text{ eV},$$

the gravitino is light (as light as a fraction of an electron-volt, the current gravitino mass limit is $\mathcal{O}(10^{-3})$) and naturally becomes the lightest supersymmetric particle (LSP) in these models. The lightest standard model superpartner, often assumed to be the lightest neutralino ($\tilde{\chi}_1^0$), is the next-to-lightest supersymmetric particle (NLSP). It becomes unstable and decays into a photon plus a gravitino ($\tilde{\chi}_1^0 \rightarrow \gamma\tilde{G}$) if $\tilde{\chi}_1^0$ has a non-zero photino component (as often the case). This type of models have been proposed for sometime [4] though much of the recent speculative theoretical attention is sparked by a single CDF event [5]. In contrast, the supersymmetry breaking scale of the gravity-mediated models is general of $\Lambda \sim 10^9$ TeV, resulting a massive gravitino which has no role in low energy supersymmetry.

In the framework of the minimal supersymmetric standard model (MSSM), the gaugino-higgsino sector is parameterized by the four parameters: M_1, M_2, μ and $\tan\beta$, where M_1 and M_2 are the $U(1)$ and $SU(2)$ gaugino mass parameters at the electroweak scale, μ is the higgsino mass parameter and $\tan\beta$ is the ratio of the vacuum expectation values of the two higgs doublets. With the gaugino mass unification at the GUT scale which is assumed here, the M_1 and M_2 have the following relationship: $M_1 = \frac{5}{3}\tan^2\theta_{\mathrm{W}} M_2$. There are four neutralinos ($\tilde{\chi}_i^0,\ i = 1,2,3,4$) and two charginos ($\tilde{\chi}_j^{\pm},\ j = 1,2$) with their masses and couplings among themself and with the Standard Model particles fixed by the three parameters (M_2, μ and $\tan\beta$) in the MSSM.

In this note, we present a direct search of the supersymmetry with a light gravitino in the framework of MSSM. We search for neutralino and chargino pair productions in $p\bar{p}$ collisions at Tevatron with R-parity conservation. In the analysis described below, the squarks and sleptons are assumed to be heavy such that the decays of charginos and neutralinos to the lightest neutralino proceed through intermediate W and Z/γ exchanges. Futhermore, the $\tilde{\chi}_1^0$ is assumed to be short-lived and to decay within the detector to $\gamma\tilde{G}$ with a branching ratio of 100%. Since the LSP is stable and non–interacting, pair production of the charginos and neutralinos will yield inclusive high E_T diphoton events with large missing transverse energy ($\not\!\!E_T$) with or without jets. The presence of high E_T photons and large $\not\!\!E_T$ provide a powerful tool for identifying these events over backgrounds.

DØ has reported a search of diphoton events with large missing transverse energy in Ref. [6], aimed at supersymmetry models with $\tilde{\chi}_1^0$ as the LSP. In this note, we present the first experimental study of the MSSM with a light gravitino as the LSP in $p\bar{p}$ collisions, motivated by several recent theoretical papers [2, 3]. Like the analysis presented in [6], no excess of events beyond the expectation of the standard processes is observed. Unlike the previous analysis, different photon identification and event selection are used, resulting in significant increase in the efficiency for supersymmetry. Bounds in the (μ, M_2) plane are derived from the search and lower limits on the $\tilde{\chi}_1^\pm$ and $\tilde{\chi}_1^0$ masses are inferred. The high efficiency enables us to set the strongest limit in the supersymmetry parameter space, exceeding those from the LEP experiments.

The rest of the note is organized as following. We briefly discuss the theoretical aspects of the chargino and neutralino pair productions first, followed by the detailed presentations of photon identification, event selection, background estimation, signal acceptance and finally the results and their interpretations. In the appendix, we compare this analysis with the analysis reported in Ref. [6].

2 Chargino and Neutralino Pair Productions

The chargino and neutralino pair productions and the subsequent $\tilde{\chi}_i^0$ and $\tilde{\chi}_j^\pm$ decays are modelled using the SPYTHIA program [7], a supersymmetric extension of the PYTHIA 5.7 program [8]. As discussed above, the cross sections are functions of supersymmetry parameters M_2, μ and $\tan\beta$ [1]. To explore the parameter space, we chose to work in the (μ, M_2) plane while keeping $\tan\beta$ fixed, a strategy used by LEP extensively for studying supersymmetric models with $\tilde{\chi}_1^0$ as the LSP. We began our studies by investigating the cross sections in the (μ, M_2) plane to minimize the time-consuming Monte Carlo simulations. Figure 1 (a) shows contours of constant cross section obtained from the SPYTHIA program for $\tan\beta = 2$. A value of $m_{\tilde{q}} = 800$ GeV/c^2 and CTEQ3L parton distribution function [9] are used in the calculation. Futhermore, the renormalization scale is set to equal to the average transverse mass of the processes. Although the productions of all possible pairs of charginos and neutralinos are included in the calculation, most of the cross section is due to $\tilde{\chi}_1^\pm\tilde{\chi}_1^\pm$ and $\tilde{\chi}_1^\pm\tilde{\chi}_2^0$ productions.

The constant mass contours of $\tilde{\chi}_1^0$ and $\tilde{\chi}_1^\pm$ are shown in Fig. 1 (b) in the same plane. Evidently, the cross section is strongly correlated with the chargino and neutralino mass. It suggests that the kinematics is largely responsible for the dependence of the cross section in the (μ, M_2) plane.

The dependence of the cross section on $\tan\beta (> 1)$ [2] is illustrated in Fig. 2 for four representative points in the (μ, M_2) parameter plane. The cross section is almost independent of $\tan\beta$ for $\tan\beta > 20$. When $\tan\beta < 20$, it increases for $\mu < 0$ and decreases for $\mu > 0$ slightly as an

[1]The SPYTHIA program takes M_1 instead of M_2 as an input parameter. In order to compare our results directly with those from LEP experiments, a small modification is made to the program to use M_2 as the input parameter with the consent of the author of the program.

[2]Since the top quark is much heavier than the bottom quark, one expects $\tan\beta > 1$. Futhermore, if the top quark Yukawa coupling remains perturbative up to the GUT scale, then $\tan\beta > 1.2$ [10]. The restriction $\tan\beta > 1$ is imposed in this analysis, but it is worth noting that the chargino and neutralino masses and couplings are symmetric under the transformation $\tan\beta \to \cot\beta$.

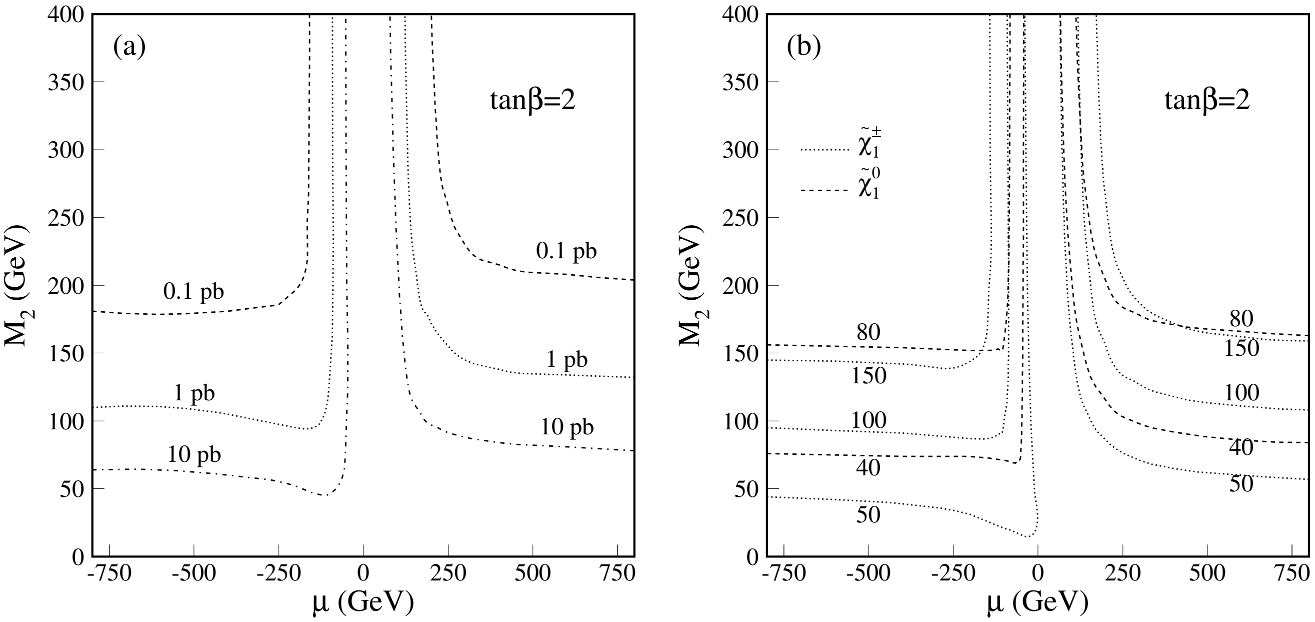

Figure 1: The constant contours in (μ, M_2) plane for $\tan\beta = 2$ of the cross section for the sum of $\tilde{\chi}_i^0\tilde{\chi}_j^0$, $\tilde{\chi}_i^0\tilde{\chi}_j^\pm$, and $\tilde{\chi}_i^\pm\tilde{\chi}_j^\mp$ production and (b) the mass of the lightest chargino (dot line) and the lightest neutralino (dash line) in the unit of GeV/c^2.

increasing $\tan\beta$. The variation in the cross section is strongly correlated with the variations in the chargino and neutralino masses. Unless it is otherwise specified, a $\tan\beta = 2$ is used in this analysis. Through t–channel diagrams, squarks also play a role in chargino and neutralino pair production. However, unless the squarks are lighter than $\sim$ 200 GeV/c^2, the effect is very small. In this analysis, we assume squark mass ($m_{\tilde{q}}$) degeneracy and set $m_{\tilde{q}}$ to be 800 GeV/c^2 which generally yields the lowest cross sections for a reasonable variation of the squark mass.

Event selection are best optimized by examining the expected distributions from the supersymmetry. The generator–level E_T distributions of the leading (γ_1) and the second (γ_2) photon expected from an integrated luminosity of 100 pb^{-1} are shown in Fig. 3 (a) for two points in the (μ, M_2) plane. No event selection is applied. The photon E_T distributions vary widely from one point to another point in the parameter space and are strongly correlated with the chargino and neutralino masses. The photon pseduorapidity distributions for the same two points are shown in Fig. 3 (b). The two distributions are normalized to an equal area. Most photons are centrally produced, in particular when charginos/neutralinos are heavy.

Topological distributions such as the diphoton opening angle and the smallest angle between '$\not{E}_T$' and the two photons in $r-\phi$ plane are shown in Fig. 4 (a) and (b) respectively, where the '$\not{E}_T$' is defined as the transverse energy of the two gravitinos. Events in these plots are required to have $E_T^{\gamma_1} > 20$ GeV, $E_T^{\gamma_2} > 12$ GeV and '$\not{E}_T$'$>$ 25 GeV. Moreover, both photons must be within $|\eta| < 2.0$. Not surprisingly, these topological distributions strongly depend on the values of the supersymmetry parameters. For example, the $\Delta\phi$ distribution peaks strongly towards 180° when chargino/neutralino are light, expected from the Lorentz boost and is almost flat

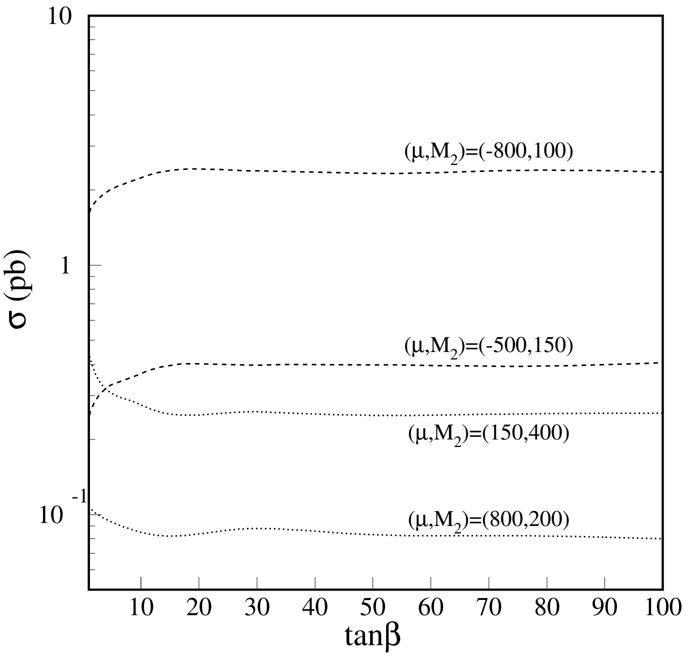

Figure 2: The cross sections as functions of $\tan\beta(> 1)$ for four representative points in the (μ, M_2) parameter plane.

when chargino/neutralino are heavy and their mass difference is small. For the same reason, the '$\not\!\!E_T$' tends to point to the direction of one of the two photons when charginos/neutralinos are light. Therefore, to maximize the sensitivity to supersymmetry in a large parameter space, topology based selection is undesired given the wide difference in topologies across the space.

3 The Analysis

The data used in this analysis were collected with the DØ detector during the 1992–1995 Tevatron Run 1A, 1B and 1C at a center–of–mass energy of 1.8 TeV. Runs with Main Ring active are vetoed using the MRBS_LOSS and MICROBLANK for Run 1B and 1C and only the MICROBLANK for Run 1A. The total effective luminosity used in this analysis is 106.3 ± 5.6 pb^{-1}. The DØ detector consists of a central tracking system, a calorimeter, and muon chambers. With the hermetic and uniform rapidity coverage of the calorimeter, the DØ detector is well suited for searching for new physics with large missing transverse energy. A detailed description of the DØ detector can be found in Ref. [11].

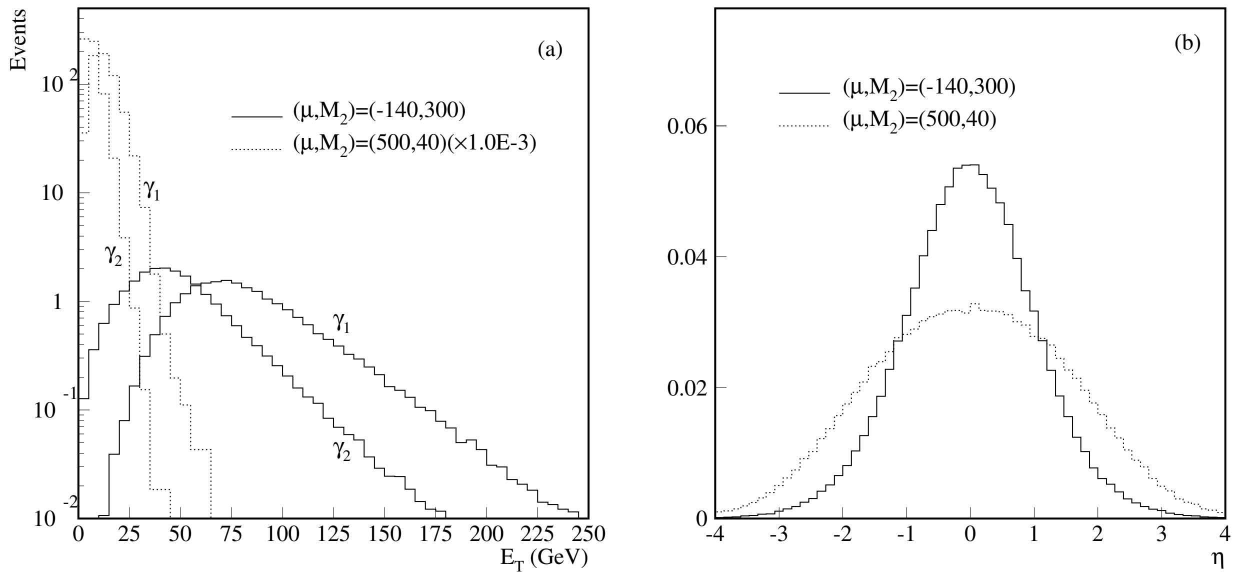

Figure 3: The generator–level E_T distributions of the leading (γ_1) and the second (γ_2) photons (a) and photon pseudorapidity distributions (b) for the two points in the parameter space without any selection. The lightest chargino and neutralino masses are (149,131) GeV/c^2 for the point $(-140, 300)$ GeV and (30,15) GeV/c^2 for the point $(500, 40)$ GeV. Note that the E_T distribution for the point (500,40) GeV has been scaled down by a factor of 1000.

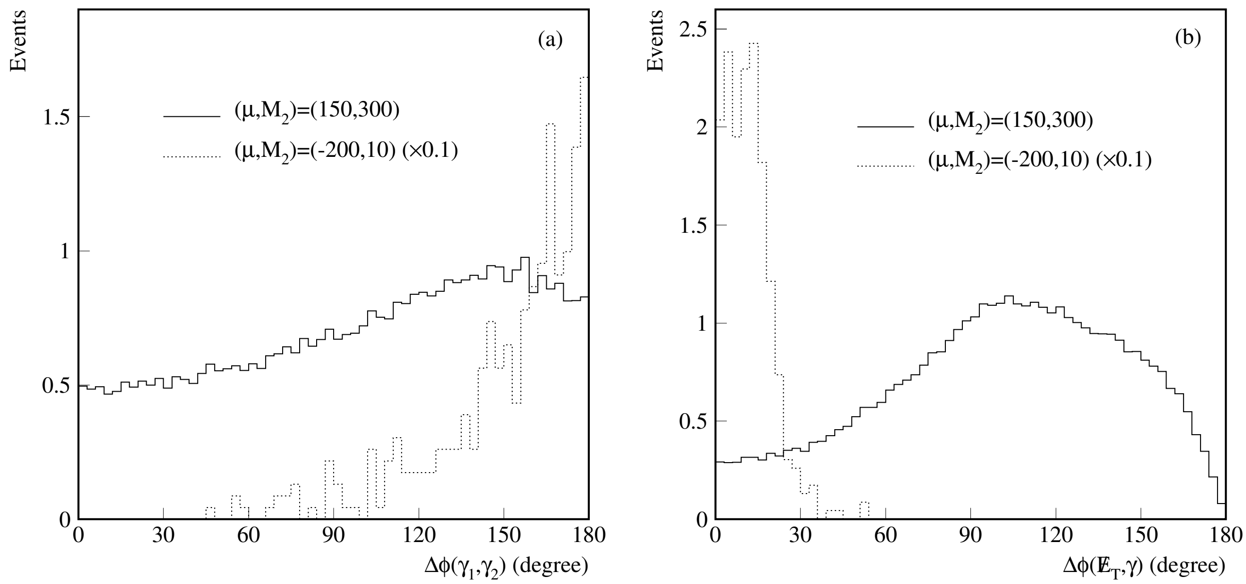

Figure 4: Topological distributions of (a) the diphoton opening angle and (b) the smallest angle between photon and '$\not{E}_T$' in $r - \phi$ plane for events passed the generator–level selection. The corresponding $(m_{\tilde{\chi}_1^\pm}, m_{\tilde{\chi}_1^0})$ are (120,93) GeV/c^2 for the point (150,300) GeV and are (31,6) GeV/c^2 for the point $(-200, 10)$ GeV. Note that the distributions for the point $(-200, 10)$ GeV have been scaled down by a factor of 10.

3.1 Photon Identification

Photons are identified by the detection of an isolated electromagnetic shower in the calorimeter and by the absence of tracking chamber hits in a road between the calorimeter shower and the event vertex.

3.1.1 Calorimeter Selection

The criteria used to select electromagnetic clusters are

(1) H–matrix $\chi^2 < 100$
The H–matrix χ^2 is a measure of the likeliness of shower profiles (transverse and longitudinal) being consistent with those expected from the electromagnetic showers.

(2) Isolation < 0.1
The isolation is defined to be the ratio between the energy in an annular isolation cone from radius 0.2 to 0.4 around the cluster in $\eta - \phi$ space and the energy of the cluster.

(3) EM fraction > 0.95
The EM fraction is the fraction of the cluster energy deposited in the electromagnetic section of the calorimeter.

These identification criteria are the same as those used in the top analyses and are discussed in detail in [13]. The efficiency (ϵ_C) for identifying electromagnetic clusters on the reconstructed PELC/PPHO's is found to be independent of cluster E_T for $E_T > 20$ GeV. Below 20 GeV, the efficiency tends to decrease with decreasing cluster E_T. The E_T dependence for $E_T < 20$ GeV has been studied in detail and is parameterized as [14]:

$$\epsilon_C(E_T) = \epsilon_C(20)(a + bE_T + cE_T^2)$$

where $\epsilon_C(20)$ are the efficiencies for identifying electromagnetic clusters with $E_T > 20$ GeV and a, b, and c are parameterization constants which are $-0.1720,\ 0.1023,\ -2.234 \times 10^{-3}$ for CC and are $0.6660,\ 0.0219,\ -3.211 \times 10^{-4}$ for EC. As presented in [13], $\epsilon_C(20)$ is 0.92 ± 0.008 for CC ($|\eta| < 1.2$) and 0.89 ± 0.017 for EC ($1.5 < |\eta| < 2.0$). An additional 2% systematic uncertainty is assigned to the efficiency for photons with $E_T < 20$ GeV to take into account the uncertainty in the parameterization.

3.1.2 Tracking Selection

Photons are further selected from the identified electromagnetic clusters using the track information and the hits-in-road information as computed by the HITSINFO package [15], originally developed for the analysis of triple gauge boson couplings [16]. Photon candidates are selected from the PPHO objects for the data and from the PELC/PPHO objects for the Monte Carlo events. The HITSINFO package searches for tracking chamber hits in a narrow angular road as defined in Table 1 between the calorimeter cluster and all reconstructed vertices. It computes the following HITSINFO variables:

RHVTXW – percentage of VTX wires hit in road

NHVTX3D – number of VTX 3d hits in road

RHCDCW – percentage of CDC wires hit in road

NHCDCXY – number of CDC XY hits in road

NHCDC3D – number of CDC 3d hits in road

NHCDCZS – number of CDC z-segments in road

RHFDCW – percentage of FDC wires hit in road

NHFDCXY – number of FDC XY hits in road

Table 2 lists the criteria imposed on these variables to select photon candidates. These requirements are identical to those used in [17]. The efficiency (ϵ_H) of non-track and the HITSINFO requirements for selecting photons in the data is obtained using the 'emulated' photon sample. This sample is obtained by rotating the calorimeter cluster position of the $Z \to ee$ electrons by $\pi/2$. To truely model the effects of underlying events, the Z+jets events are rejected by requiring the $r - \phi$ opening angle of the two electrons to be greater than 170°. The efficiency loss due to the random track overlap in the tracking road is taking into account by rejecting any rotated calorimeter cluster which is reconstructed as a PELC after redoing the track reconstruction. A new tighter road is constructed between the surviving emulated photon cluster and the vertex. All the HITSINFO variables are recomputed using this new rotated cluster, the efficiency is then the fraction of 'emulated photons' passing the HITSINFO selection. This procedure mimics the situation of real photons, and take care of any random tracks in road and other multiple interaction and instataneous luminosity effects. The $Z \to ee$ event for this study have the invariant mass within 5 GeV window of M_Z (86-96 GeV). This reduces the number of background events in our sample. The efficiency of the track and the HITSINFO selections for photons obtained this way is 0.78 ± 0.02 ($\sim$ 89% due to overlap tracks and $\sim$ 88% due to HITSINFO) due to the HITSINFO selection) for CC photons and 0.80 ± 0.05 for EC photons [3].

Detector	$\Delta\theta$ (rad)	$\Delta\phi$ (rad)
CDC	0.05	0.0075
VTX	0.005	0.012
FDC	0.005	0.015

Table 1: The angular road used by the HITSINFO package to count numbers of hits in the three tracking detectors.

[3]The efficiency (0.90 ± 0.04) reported in [17] is for HITSINFO selection only. It does not take into account the efficiency loss due to the track overlaps.

RHVTXW < 0.3	
NHVTX3D ≤ 8	
CDC	FDC
RHCDCW < 0.3	RHFDCW < 0.7
NHCDCXY ≤ 20	NHFDCXY ≤ 30
NHCDC3D ≤ 1	
NHCDCZS $= 0$	

Table 2: The HITSINFO selection applied on the electromagnetic clusters to identify photon candidates. These requirements are identical to those used in [17].

3.1.3 Photon Conversions

A photon would not be identified if it interacts in the material in front of the tracking chambers. The photon conversion probability is estimated using single photon Monte Carlo events. The Monte Carlo sample was GEANTed using full showering and reconstructed with the latest DØRECO version. The calculated conversion probability as a function of pseduorapidity is shown in Fig. 5. The average efficiency loss $(1-\epsilon_X)$ due to photon conversion is pseduorapidity-dependent and is about 10% in CC and 30% in EC. The estimated systematic error is about 10% of the conversion probability.

The combined identification efficiencies ϵ_γ ($=\epsilon_C \times \epsilon_H \times \epsilon_X$) from the reconstructed PPHO clusters with $E_T > 20$ GeV are about 75% in CC and 60% in EC. The efficiencies for photons with $E_T < 20$ GeV are E_T dependent and the functional forms discussed above are used in the analysis.

3.1.4 Electron Rejection

Due to the imperfect tracking detector and tracking algorithm, an electromagnetic cluster produced by an electron can be misidentified as a photon. To aid the background estimation discussed in Sec. 3.3, we introduce an electron rejection factor (R) which is defined as the ratio between the numbers of electrons and photons identified from a sample of electron–originated electromagnetic clusters. Unless otherwise specified, electrons are selected from PELC objects and must pass the criteria for the electromagnetic clusters and have track–match significances ($\sigma_{\rm TM}$) less than 5. The rejection is calculated using the same method described in Ref. [16]. It consists of two components: rejection provided by the track (by only considering PPHO objects as photon candidates) and the rejection provided by the HITSINFO selection.

The rejection from the track (R_T) is calculated using the tracking finding efficiency (ϵ_t) and the efficiency (ϵ_m) for track–match significance requirement reported in [13] using the formula:

$$R_T = \frac{\epsilon_t \epsilon_m}{1-\epsilon_t}.$$

It is found to be 6.1 ± 0.3 for CC and 4.7 ± 0.2 for EC for the efficiencies ($\epsilon_t = 0.864 \pm 0.014$,

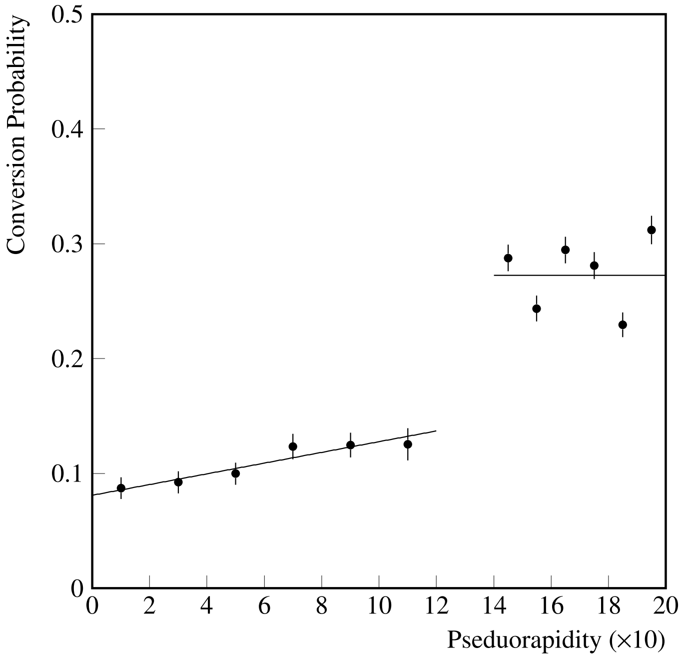

Figure 5: Photon conversion probability as a function of pseudorapidity. The errors are statistical only. The systematic error is estimated to be about 10% of the conversion probability.

$\epsilon_m = 0.934 \pm 0.009$ for CC and $\epsilon_t = 0.861 \pm 0.018$, $\epsilon_m = 0.766 \pm 0.028$ for EC) presented in [13]. The rejection of the HITSINFO selection in DØRECO version 12.20 or higher is estimated using the loose $W \rightarrow$'e'ν events. This sample is selected by requiring one PPHO cluster passing the electromagnetic identification and with $E_T > 20$ GeV. In addition, the events are required to have $\not\!\!E_T > 25$ GeV. The HITSINFO selection is then applied to the sample. After subtracting QCD backgrounds from the sample both before and after HITSINFO selection, rejection factors (R_H) of 37.5 ± 5.9 for CC and 35.9 ± 8.4 for EC are obtained. Combining the rejections of the track and the HITSINFO selection, the tracking provided a total electron rejection factor ($R = R_H \times R_T$) of 229 ± 38 for CC and 169 ± 37 for EC. These numbers are in good agreement with 245 ± 60 for CC and 160 ± 50 for EC reported in [16] for Run 1A. The HITSINFO selection in DØRECO versions earlier than 12.20 is found to be inefficient in reducing backgrounds for photons.

The validity of the HITSINFO rejection of electrons is checked using a sample of $Z \rightarrow ee$ events, which are selected by requiring two electromagnetic clusters each with $E_T > 20$ GeV and an invariant mass of the pair $86 < M_{ee} < 96$ GeV/c^2. The electromagnetic cluster can either be a PELC or a PPHO object. The HITSINFO rejection is then obtained by imposing the selection to the PPHO clusters. The rejection factor obtained for the CC is 40 ± 7, in good agreement with that estimated using the loose W events.

3.2 Event Selection

This analysis is restricted to events from the Level 2 filter ELE_JET for Run 1A and ELE_JET_HIGH for Run 1B/1C. The ELE_JET filter requires one electromagnetic cluster with $E_T > 15$ GeV, one 'jet' with $E_T > 10$ GeV and a missing transverse energy $\not{E}_T > 10$ GeV. In addition, both the electromagnetic cluster and the jet must have pseduorapidities $|\eta| < 2.5$. Apart from the $\not{E}_T$ requirement for which the threshold is raised to 14 GeV, the other requirements for the ELE_JET_HIGH filter are identical to those of the ELE_JET filter. For both filters, the jets in the trigger include non-leading electromagnetic clusters.

The signature of pair production of the charginos and neutralinos is two high E_T photons associated with the large missing transverse energy. As discussed above, the event topology of pair production of charginos and neutralinos is substantially different across the parameter space. Topological cuts (such as angle between two photons, $\not{E}_T$ direction etc...) will result in loss of efficiency in some region of the space. With excellent photon identification and good $\not{E}_T$ resolution, we found that simple kinematic requirements are sufficient to reduce backgrounds to a negligible level. To be selected as $\gamma\gamma\not{E}_T$ candidates, events must have two identified photons and satisfy the following kinematic requirements:

(1) $E_T^{\gamma_1} > 20$ GeV with $|\eta^{\gamma_1}| < 1.2$ or $1.5 < |\eta^{\gamma_1}| < 2.0$,

(2) $E_T^{\gamma_2} > 12$ GeV with $|\eta^{\gamma_2}| < 1.2$ or $1.5 < |\eta^{\gamma_2}| < 2.0$,

(3) $\not{E}_T > 25$ GeV.

In addition, there must be at least one reconstructed vertex in the events to ensure good measurements of the missing transverse momenta. No requirement on jets is made in the selection. The $\not{E}_T$ is determined from the energy deposition in the calorimeter with $|\eta| < 4.5$. The higher E_T requirement on the leading photon is necessitated by the trigger threshold. Nevertheless, the requirement is efficient for the parameter region with heavy charginos and neutralinos as shown, for example, in Fig. 3 (a). The pseduorapidity requirement is dictated by the detector acceptance. After these cuts, two events (one from Run 1A and the other from Run 1B) survived [4].

Since only $\sim 15\%$ of the data are processed with the good HITSINFO, events which passed all the selection above except the HITSINFO and the $\not{E}_T$ selections (229 events) are picked using the PICK_EVENTS utility and reprocessed with the good HITSINFO package. These events are referred to as the $\gamma\gamma$ events in the following discussion. Twenty-eight events survived the HITSINFO selection after reprocessing. Two of these events have $\not{E}_T$ above 25 GeV. The $\not{E}_T$ distributions before and after the HITSINFO selection are shown in Fig. 6.

[4] The Run 1A event (Run#=62433, Event#=10839) has a $\not{E}_T$ pointing to the Main Ring direction while the Run 1B event (Run#=91267, Event#=38689) has a photon in the Main Ring region and a $\not{E}_T$ back-to-back with that photon. We note that these events can be easily removed by applying additional requirements based on event topology. However, any topology based selection will undoubtly reduce the sensitivity to the events from supersymmetry.

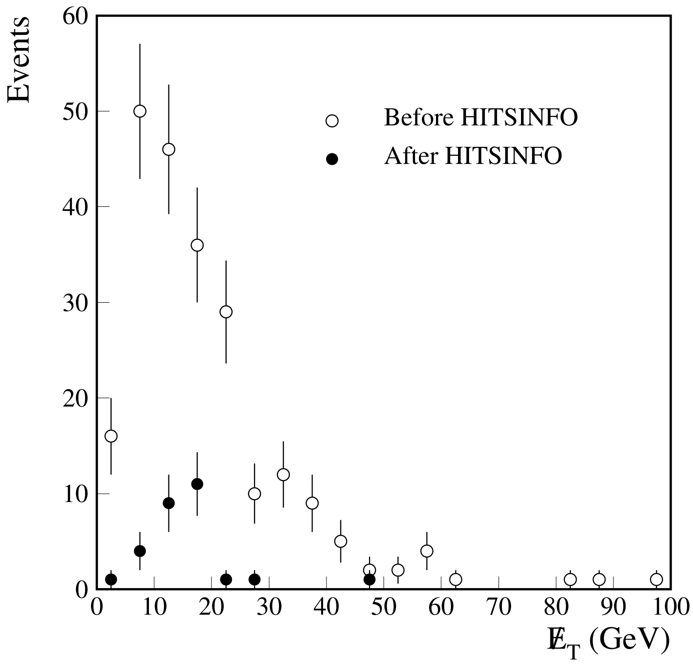

Figure 6: The $\not\!\!E_T$ distribution of diphoton events before (open circle) and after (solid circle) HITSINFO selection. After the HITSINFO selection, two events have $\not\!\!E_T$ greater than 25 GeV.

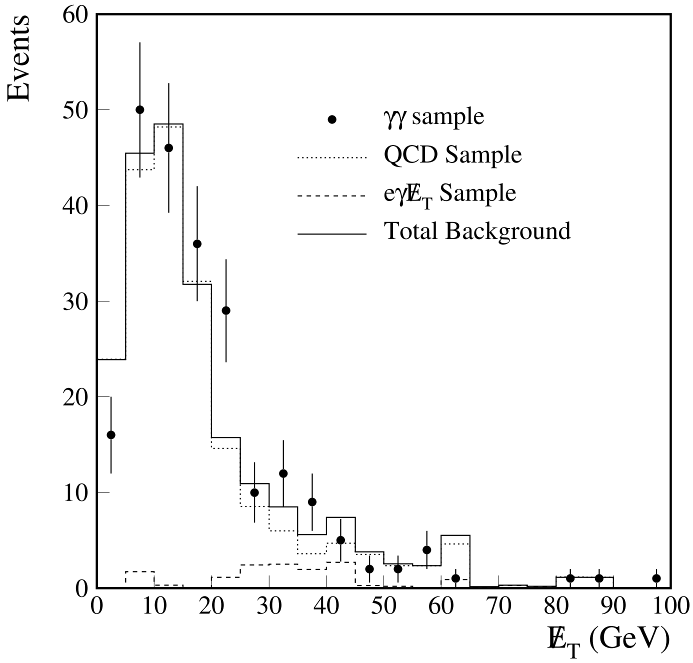

Figure 7: The $\not\!\!E_T$ distributions of the $\gamma\gamma$ and the background samples before the HITSINFO and the $\not\!\!E_T$ selections. The number of events with $\not\!\!E_T < 20$ GeV of the background samples is normalized to that of the $\gamma\gamma$ sample. The $e\gamma\not\!\!E_T$ contribution is obtained from those of the $ee, e\gamma$ events after subtracting QCD backgrounds by applying the electron rejection factor of the track (R_T). The apparent peak in the distribution is a result of falling spectrum with a trigger threshold.

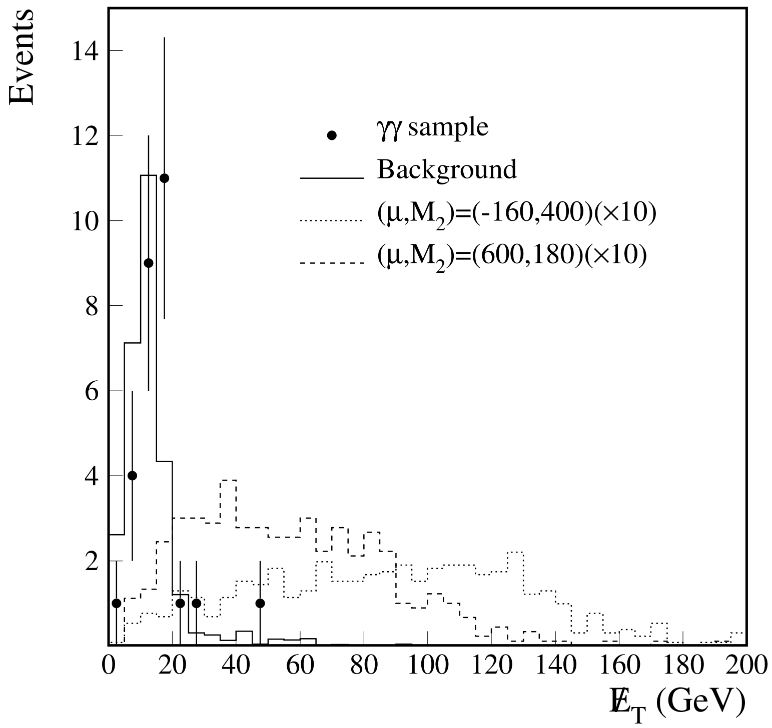

Figure 8: The $\not\!\!E_T$ distributions of the $\gamma\gamma$ and the background samples after the HITSINFO selection. Two $\gamma\gamma$ events have $\not\!\!E_T > 25$ GeV after HITSINFO selection. The number of events with $\not\!\!E_T < 20$ GeV in the background sample is normalized to that in the $\gamma\gamma$ sample. As discussed in Sec. 3.3, the $e\gamma\not\!\!E_T$ background is small after the HITSINFO selection. Also shown are the expected distributions from the supersymmetry. Note that the distributions of the supersymmetry have been scaled up by factor of ten.

3.3 Background Estimations

The multijet, direct photon, $W+\gamma$, $W+$jets, $Z \to ee$, $Z \to \tau\tau \to ee$ events from the Standard Model processes with misidentified photons and/or mismeasured $\not\!\!E_T$ are the background sources for the $\gamma\gamma\not\!\!E_T$ events. The numbers of background events from these sources are estimated using data for the following two cases: diphoton events (genuine or misidentified) without genuine $\not\!\!E_T$ and events with genuine $\not\!\!E_T$.

Genuine or misidentified diphoton events without genuine $\not\!\!E_T$ will be misidentified as $\gamma\gamma\not\!\!E_T$ events if the $\not\!\!E_T$'s are significantly mismeasured. This background is estimated using a QCD sample selected by requiring

(1) EM fraction > 0.9 for both clusters,

(2) Isolation < 0.1 for both clusters,

(3) at least one cluster with H–matrix $\chi^2 > 200$,

(4) no track in road for PPHO clusters, and

(5) track–match significance greater than 10 for PELC objects

from the same dataset with the same trigger. The EM clusters can be either PELC or PPHO objects. In addition, the events are required to pass the kinematic requirements except the cut on $\not\!\!E_T$. As discussed above, the HITSINFO selection in DØRECO versions earlier than 12.20 are inefficient in rejecting backgrounds for photons. To avoid any inconsistency, no HITSINFO selection is applied here. These events are similar to those of the $\gamma\gamma$ sample and are expected to suffer from the similar $\not\!\!E_T$ mismeasurement. For this reason, the $\not\!\!E_T$ distributions of the two samples are assumed to be the same for small $\not\!\!E_T$ in the analysis. They are compared in Fig. 7. Using a subset of the QCD sample processed with DØRECO version 12.20 or higher, the fraction of events passing the HITSINFO selection is computed as a function of $\not\!\!E_T$. Convoluting the fraction to the $\not\!\!E_T$ distribution of the QCD sample before the HITSINFO, a $\not\!\!E_T$ distribution of the QCD sample after the HITSINFO is obtained. By normalizing the number of events with $\not\!\!E_T <$ 20 GeV in the QCD sample to that in the $\gamma\gamma$ sample (see Fig. 8), a background of 2.1 ± 0.9 events due to the $\not\!\!E_T$ mismeasurement is obtained for $\not\!\!E_T >$ 25 GeV.

The other backgrounds are due to events with genuine $\not\!\!E_T$ such as those from $W+$'γ' (where 'γ' can be a real or a fake photon), $Z \to \tau\tau \to ee$ and $t\bar{t} \to ee+$jets productions. These events (labelled as $e\gamma\not\!\!E_T$ events) would fake $\gamma\gamma\not\!\!E_T$ events if electrons are misidentified as photons. Their contribution is estimated from the data with electrons. A sample of e'γ' events (29 events in CC and 8 events in EC) passing the kinematic requirements including that on $\not\!\!E_T$ is selected. Standard electron and photon identifications are applied to select these events. By applying the electron rejection factors discussed in Sec. 3.1.4, an estimated 0.2 ± 0.1 events is expected.

Figure 7 compares the $\not\!\!E_T$ distributions of the $\gamma\gamma$, the QCD and the $e\gamma\not\!\!E_T$ samples before the HITSINFO selection. The number of events in the background samples is normalized to the corresponding number in the $\gamma\gamma$ sample. The $e\gamma\not\!\!E_T$ distribution is obtained by adding the distributions of ee events scaled down by a factor of R_T^2 and $e\gamma$ events scaled down by a factor of R_T after background subtractions. The ee and $e\gamma$ events are selected using the above kinematic requirement except the cut on $\not\!\!E_T$.

Adding the two background contributions together, a total 2.3 ± 0.9 background events is expected.

3.4 Signal Acceptances

Based on the theoretical cross sections of chargino and neutralino pair productions and acceptance studies at the generator–level, we have generated and simulated $\tilde{\chi}_i^0\tilde{\chi}_j^0$, $\tilde{\chi}_i^0\tilde{\chi}_j^\pm$ and $\tilde{\chi}_i^\pm\tilde{\chi}_j^\pm$ events for a large number of points in the (μ, M_2) parameter space. The Monte Carlo events are required to pass a GEANT [12] based DØ detector simulation program and a trigger simulator. They are subjected to the DØRECO version 12.22. For simplicity, the decay $\tilde{\chi}_1^0 \to \gamma\tilde{G}$ is assumed to occur close to the event vertex in the simulation and the gravitino mass is set to zero. Table 3 lists the points in the (μ, M_2) parameter plane for $\tan\beta = 2$ with GEANT simulations together with the corresponding masses of the lightest chargino and neutralino and the theoretical cross sections obtained from the SPYTHIA program. The cross section is calculated using the CTEQ3L parton distribution function [9], but is found to be insensitive to the choice of the parton distribution functions. The renormalization scale is set to the average transverse mass of the processes in the calculation.

The total efficiency for the supersymmetry and its breakdowns are listed in Table 3. The followings are brief definitions of the efficiencies:

- ϵ_K parton-level efficiency of kinematic requirements on photons and $\not{E}_T$;
- ϵ_R reconstruction efficiency;
- ϵ_T trigger efficiency (not listed in the table);
- ϵ_{ID} identification efficiency for both photons: $\epsilon_{ID} = (\epsilon_C \times \epsilon_H \times \epsilon_X)^2$.
- ϵ total efficiency for the supersymmetry: $\epsilon = \epsilon_K \times \epsilon_T \times \epsilon_R \times \epsilon_{ID}$.
- ϵ_D detecting efficiency for events passing kinematic requirements on photons and $\not{E}_T$: $\epsilon_D = \epsilon_T \times \epsilon_R \times \epsilon_{ID}$.

The trigger efficiency estimated using the trigger simulator for events which passed kinematic cuts ranges from 90% for light chargino/neutralino to almost 100% for heavy charginos/neutralinos. The photon identification efficiency includes the efficiencies of the calorimeter and tracking based selections as well as the efficiency loss due to the conversion of the photons to electrons. It also takes into account the over-estimation of the efficiency loss in the CCEM $\phi-$crack by the SHOWERLIB version of the GEANT. By comparing the ϕ distribution (after mapping back onto a single CCEM module) of electromagnetic clusters between the data (W events) and the Monte Carlo (signal events), it is estimated that the inefficiency due to the $\phi-$crack is over-estimated by $(5 \pm 3)\%$ per object by the SHOWERLIB. The total efficiency for the supersymmetry varies greatly from $\sim 0.01\%$ to $\sim 26\%$, depending largely on the masses of $\tilde{\chi}_1^{\pm}$ and $\tilde{\chi}_1^0$ and their mass difference. The estimated systematic error on the total efficiency is 6% which includes the efficiency uncertainties of the electromagnetic cluster identification (3%), the HITSINFO selection (3%), the reconstruction (2%), the photon conversions (2%), and the CCEM $\phi-$crack modeling (4%).

Sample distributions of the Monte Carlo events which passed the event selection for the two selected points in the (μ, M_2) plane are shown in Fig. 9. All distributions are normalized to the expected numbers of events after the selection in our sample. The jets are reconstructed using a cone algorithm of radius $\sqrt{(\Delta\phi)^2 + (\Delta\eta)^2} = 0.5$ and are required to have $E_T > 15$ GeV and $|\eta| < 2.0$. As shown in the Fig. 9 (c), the opening angle between $\not{E}_T$ and the leading photon is large, a topology expected from heavy $\tilde{\chi}_1^0$ decays. Also the distribution of the smallest opening angle between $\not{E}_T$ and jets in $r-\phi$ is flat when $m_{\tilde{\chi}_1^{\pm}} - m_{\tilde{\chi}_1^0}$ is large and favors large angles when

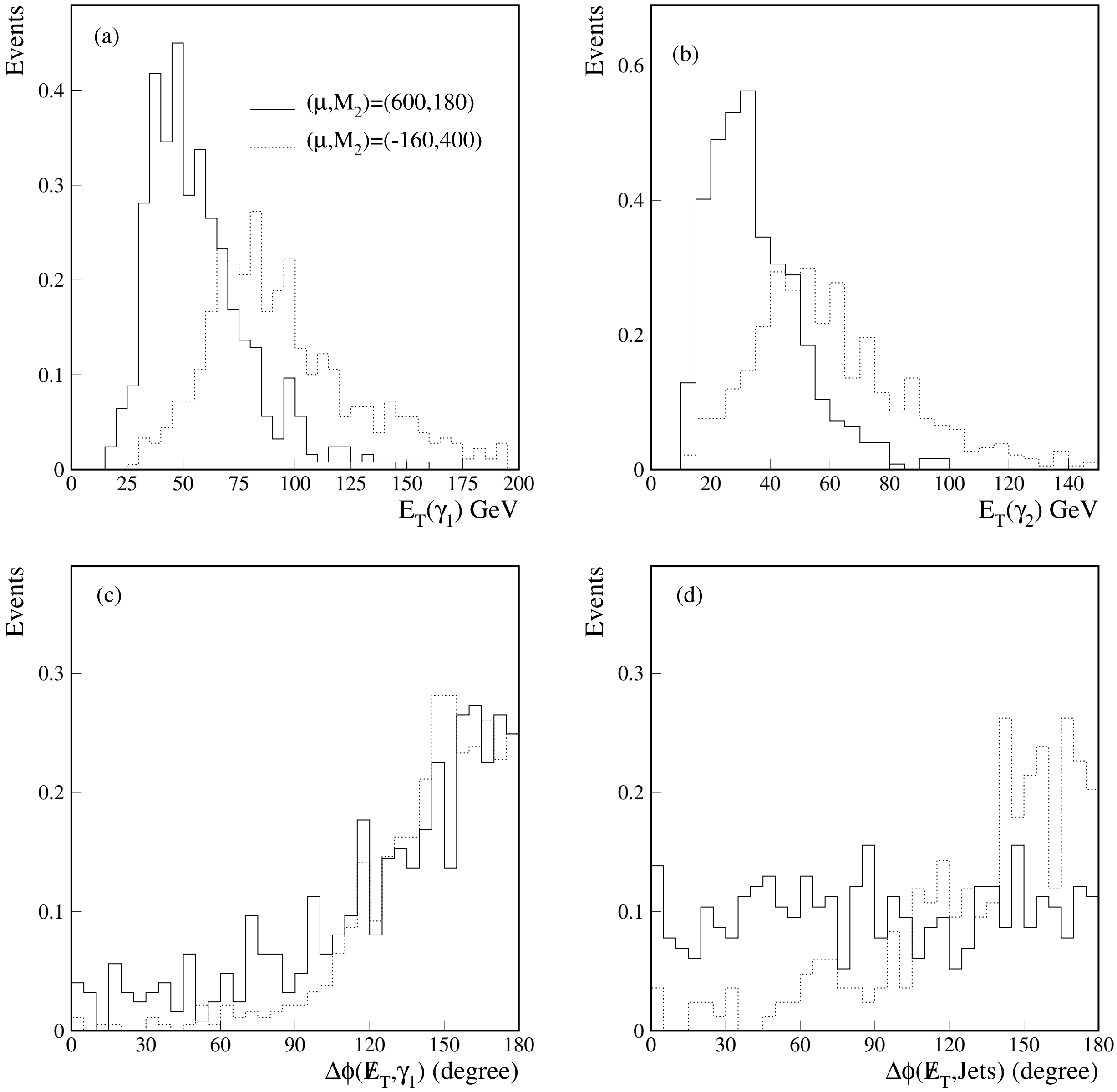

Figure 9: The Monte Carlo distributions of (a) the leading photon E_T, (b) the second photon E_T, (c) the opening angle between $\not\!\!E_T$ and the leading photon in $r-\phi$ plane, and (d) the smallest angle between $\not\!\!E_T$ and jets in $r-\phi$ plane for the two points in the supersymmetry parameter space. The corresponding $(m_{\tilde{\chi}_1^\pm}, m_{\tilde{\chi}_1^0})$ are (167,154) GeV/c^2 for the point $(-160,400)$ GeV and are (168,87) GeV/c^2 for the point (600,180) GeV. All distributions are normalized to the expected numbers of events in the data.

μ GeV	M_2 GeV	$m_{\tilde{\chi}_1^0}$ (GeV/c^2)	$m_{\tilde{\chi}_1^\pm}$	σ_{th} (pb)	Efficiency (%) ϵ_K	ϵ_R	ϵ_{ID}	ϵ_D	$\epsilon(=\epsilon_K\epsilon_D)$	σ_D (pb)	σ (pb)
−10	10	6.2	51.4	985	0.062		40.8	–	0.025±0.008	–	286
−10	300	8.7	25.5	3458	0.072		38.5	–	0.029±0.008	–	223
−10	500	8.9	19.8	3810	0.022		36.6	–	0.008±0.004	–	477
−100	10	6.1	42.3	974	0.026		52.0	–	0.014±0.003	–	391
−200	10	6.1	31.4	4822	0.020		51.9	–	0.010±0.002	–	540
−145	300	134.6	153.6	0.19	67.7	86.6	42.5	35.7	24.2±1.4	0.13	0.20
−145	400	140.2	152.9	0.19	66.9	83.3	42.9	35.1	23.5±1.3	0.14	0.21
−160	200	103.6	163.1	0.18	65.9	71.0	42.7	29.8	19.6±1.3	0.16	0.25
−160	300	143.9	167.8	0.12	71.5	85.7	42.9	36.4	26.0±1.4	0.13	0.18
−160	400	154.4	167.5	0.12	66.2	87.4	42.9	37.0	24.5±1.4	0.13	0.20
−160	500	156.5	166.8	0.12	66.0	91.7	42.8	38.1	25.2±1.4	0.13	0.19
−180	200	103.9	177.4	0.13	62.3	76.5	42.6	32.3	20.1±1.3	0.15	0.24
−200	160	84.3	163.1	0.23	60.5	71.7	42.6	29.9	18.1±1.2	0.16	0.27
−300	160	83.7	167.8	0.19	56.1	68.0	42.1	28.4	15.9±1.2	0.17	0.30
−400	150	78.2	157.8	0.25	57.2	78.1	42.7	32.8	18.8±1.2	0.15	0.26
−400	160	83.2	167.5	0.20	58.1	68.5	42.6	28.8	16.8±1.2	0.17	0.29
−500	160	82.8	166.8	0.22	57.0	62.5	42.5	26.4	15.1±1.1	0.18	0.32
−600	140	72.5	146.4	0.36	53.5	76.8	42.6	32.1	17.2±1.2	0.15	0.28
−600	160	82.5	166.1	0.21	58.0	57.7	42.5	24.3	14.1±1.1	0.20	0.35
−800	150	77.1	155.1	0.31	58.2	77.9	42.3	32.6	19.0±1.2	0.15	0.25
−800	165	84.7	170.0	0.20	57.2	61.7	42.8	26.4	15.1±1.1	0.18	0.32
−1000	160	81.9	164.2	0.23	58.0	70.5	42.4	29.7	17.2±1.2	0.16	0.28
−1000	170	86.9	174.2	0.17	60.9	62.8	42.7	26.8	16.3±1.2	0.18	0.30
10	300	6.1	6.7	3523	0.140		51.0	–	0.078±0.008	–	65
145	500	117.4	130.4	0.39	66.1	62.8	42.5	26.0	17.2±1.2	0.18	0.28
170	500	139.0	154.2	0.18	68.3	80.4	42.8	33.9	23.2±1.4	0.14	0.21
180	300	109.7	144.4	0.24	62.3	62.1	42.4	26.2	16.3±1.2	0.18	0.30
180	350	123.2	152.1	0.18	66.0	76.9	42.8	32.7	21.6±1.3	0.15	0.22
200	300	118.1	160.2	0.15	66.8	75.5	42.6	31.9	21.3±1.3	0.15	0.23
300	190	85.6	152.4	0.28	61.3	62.6	41.9	25.7	15.8±1.2	0.19	0.31
300	205	92.9	164.0	0.19	61.6	77.0	42.4	32.4	20.0±1.3	0.15	0.24
400	190	89.4	166.4	0.19	61.7	77.2	42.8	32.5	20.1±1.3	0.15	0.24
500	185	88.6	168.5	0.19	62.2	76.4	42.6	31.9	19.9±1.3	0.15	0.24
600	175	84.6	162.6	0.24	61.8	63.1	42.3	26.4	16.3±1.2	0.18	0.30
600	180	87.1	167.5	0.20	59.5	68.9	42.4	28.8	17.2±1.2	0.17	0.28
800	170	83.2	161.6	0.25	58.7	79.8	42.5	33.4	19.6±1.3	0.14	0.25
1000	170	83.8	163.6	0.24	62.3	72.1	42.2	29.8	18.5±1.2	0.16	0.26

Table 3: Shown is a list of points in the (μ, M_2) plane for $\tan\beta = 2$ with GEANT simulation. The errors on the total efficiencies are statistical only. The systematic errors are estimated to be 6%. The last two columns list the 95% CL upper limits on the detectable (σ_D) and the total (σ) cross sections.

$m_{\tilde{\chi}_1^\pm} - m_{\tilde{\chi}_1^0}$ is small as expected from the decay kinematics. In the case of small $m_{\tilde{\chi}_1^\pm} - m_{\tilde{\chi}_1^0}$, there is little jet activity in the events (see Fig. 10). In this case, most of the energy in an event is carried by photons and gravitinos, resulting in hard photon E_T spectra as demonstrated in Fig. 9 (a) and (b) and $\not{E}_T$ distribution shown in Fig. 8.

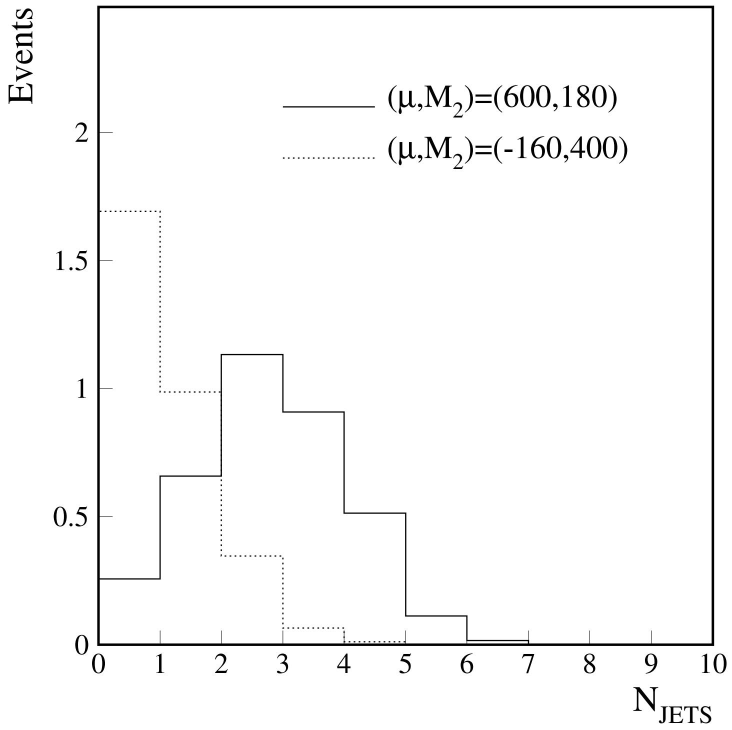

Figure 10: The distributions of the number of jets expected from pair productions of charginos and neutralinos for the two points in the (μ, M_2) plane.

3.5 Comments on $\not{E}_T$ Requirement

Large missing transverse energy is a key signature for the productions of the supersymmetric particles while most of background events from the standard model processes have zero or small $\not{E}_T$. Therefore, it is important to understand the cut on $\not{E}_T$. Table 4 [5] shows the numbers of candidate and background events together with the expected efficiencies of the supersymmetry for the two representative points in the parameter space. As expected, the number of background events and the efficiency for the supersymmetry decrease as the $\not{E}_T$ threshold increases. A 25 GeV $\not{E}_T$ threshold is used in many previous analyses to select $W \to e\nu$ events and is adopted in this analysis. As shown in the table, it represents a reasonable compromise between the efficiency and the background.

[5] $e\gamma\not{E}_T$ events with $\not{E}_T < 20$ GeV are not picked for reprocessing with the good HITSINFO package. Therefore, no background estimation is made.

$\not\!\!E_T$ Threshold	Candidates $N_{\gamma\gamma}$	Backgrounds QCD Sample	$e\gamma\not\!\!E_T$ Sample	Efficiencies $(-160, 400)$	$(600, 180)$
> 20 GeV	3	3.3 ± 1.4	$--$	0.256	0.184
> 25 GeV	2	2.1 ± 0.9	0.18 ± 0.09	0.247	0.172
> 30 GeV	1	1.4 ± 0.7	0.12 ± 0.07	0.241	0.160
> 35 GeV	1	1.0 ± 0.6	0.12 ± 0.07	0.238	0.149

Table 4: Numbers of $\gamma\gamma\not\!\!E_T$ and background events for four different thresholds on the $\not\!\!E_T$. The efficiencies of the supersymmetry for the two representative points are also shown.

4 Results and Discussions

4.1 Cross Section Limits

With two events observed and 2.3 ± 0.9 events expected from the backgrounds, we observe no excess of events above the expectation from the misidentifications and mismeasurements. We compute 95% C.L. upper limits of the total cross section (σ) for the sampling points in the (μ, M_2) plane using the estimated efficiencies (ϵ) with their errors discussed above. The σ computed using a Bayesian approach [18] with a flat prior distribution for the signal cross section are listed in the last column of the Table 3. Depending on the values of the supersymmetry parameters, the limits vary widely from a few hundreds pb for light charginos/neutralinos to ~ 0.18 picobarn for heavy charginos/neutralinos.

We also compute 95% C.L. upper limits of the detectable cross section (σ_D) for diphoton events with $E_T^{\gamma_1} > 20$ GeV, $E_T^{\gamma_2} > 12$ GeV, $|\eta^\gamma| < 1.2$ or $1.5 < |\eta^\gamma| < 2.0$, and $\not\!\!E_T$>25 GeV using the detecting efficiency ϵ_D for the parameter points of interests. The resulting limits are also listed in Table 3. The limits vary from ~ 0.13 pb to ~ 0.20 pb, depending on the value of the supersymmetry parameters. Conservatively, we set a 95% CL detectable cross section limit for inclusive pair production of charginos and neutralinos $\sigma_D < 0.20$ pb for diphoton events with $E_T^{\gamma_1} > 20$ GeV, $E_T^{\gamma_2} > 12$ GeV, $|\eta^\gamma| < 1.2$ or $1.5 < |\eta^\gamma| < 2.0$, and $\not\!\!E_T$> 25 GeV. Care must be taken in comparing this limit with that reported in Ref. [6] due to different kinematic cuts applied. Parton level studies show that the kinematic cuts used in this analysis is about 30% more efficient than those used in Ref. [6]. Moreover, the Monte Carlo events used to calculate the efficiency in this analysis is generally more jetty than those of used in Ref. [6]. Please also note that this limit is somewhat arbitrary given that only a limited number of parameter points are sampled.

4.2 Bounds in the Supersymmetry Parameter Space

To derive limits in the (μ, M_2) plane, the values of μ and M_2 are varied around the sampled points till the theoretical cross sections exceed the upper limits. The bounds in the (μ, M_2) plane are shown in Fig. 11 along with the points sampled with GEANT simulations. As shown

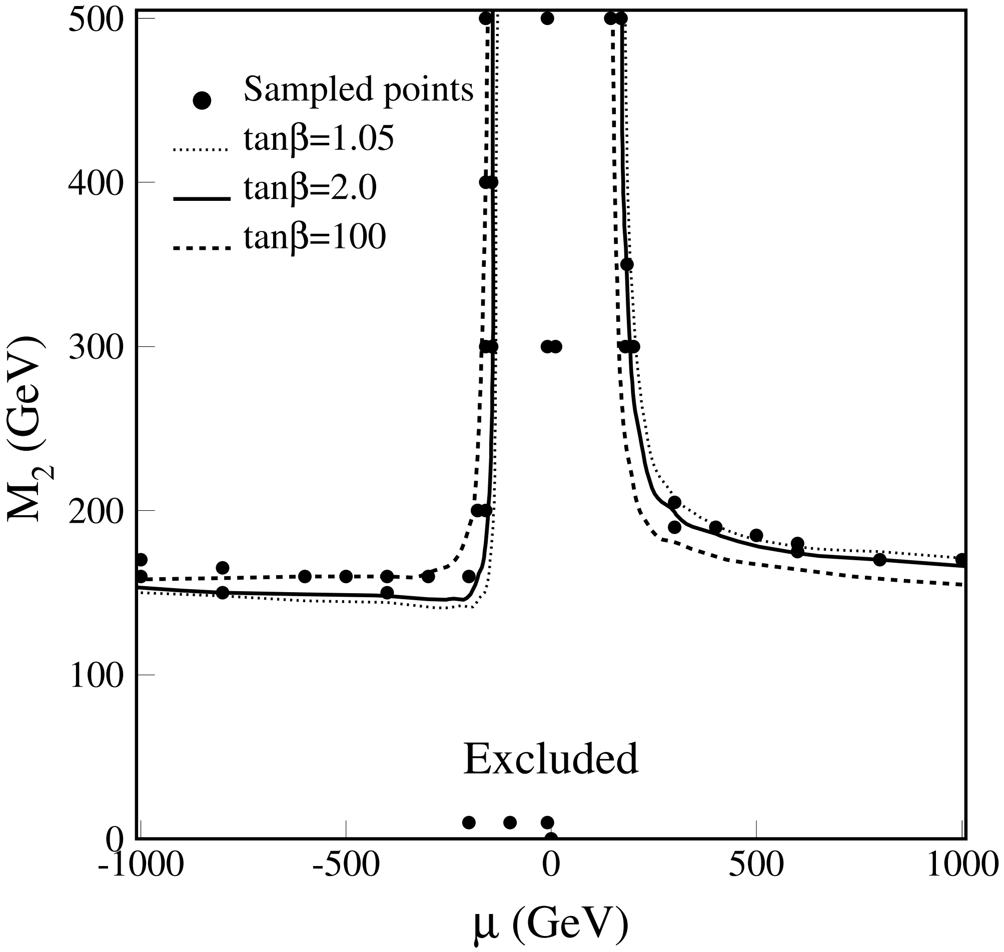

Figure 11: Sampled points in the (μ, M_2) plane with GEANT simulation. Also shown are bounds for $\tan\beta = 2$ (solid line), $\tan\beta = 1.05$ (dotted line) and $\tan\beta = 100$ (dashed line) derived from this analysis.

in Table 3, the efficiency for the supersymmetry is reasonable constant around the sampled points when the charginos and neutralinos are heavy, despite of the great variations across the parameter space. Here a constant efficiency for the supersymmetry is assumed around a sampled point. Furthermore, the smaller of the two efficiencies is used when two points are close together in the parameter space. The parameter region below the two solid lines are excluded by the analysis for $\tan\beta = 2$. The bounds depend on the $\tan\beta$ value slightly. In general, the bounds are stronger in the $\mu < 0$ half–plane and are weaker in the other half–plane for a larger $\tan\beta$. The bounds for a smaller $\tan\beta$ are almost identical to those of $\tan\beta = 2$. The limits for $\tan\beta = 1.05$ and $\tan\beta = 100$ are shown in Fig. 11 for comparisons.

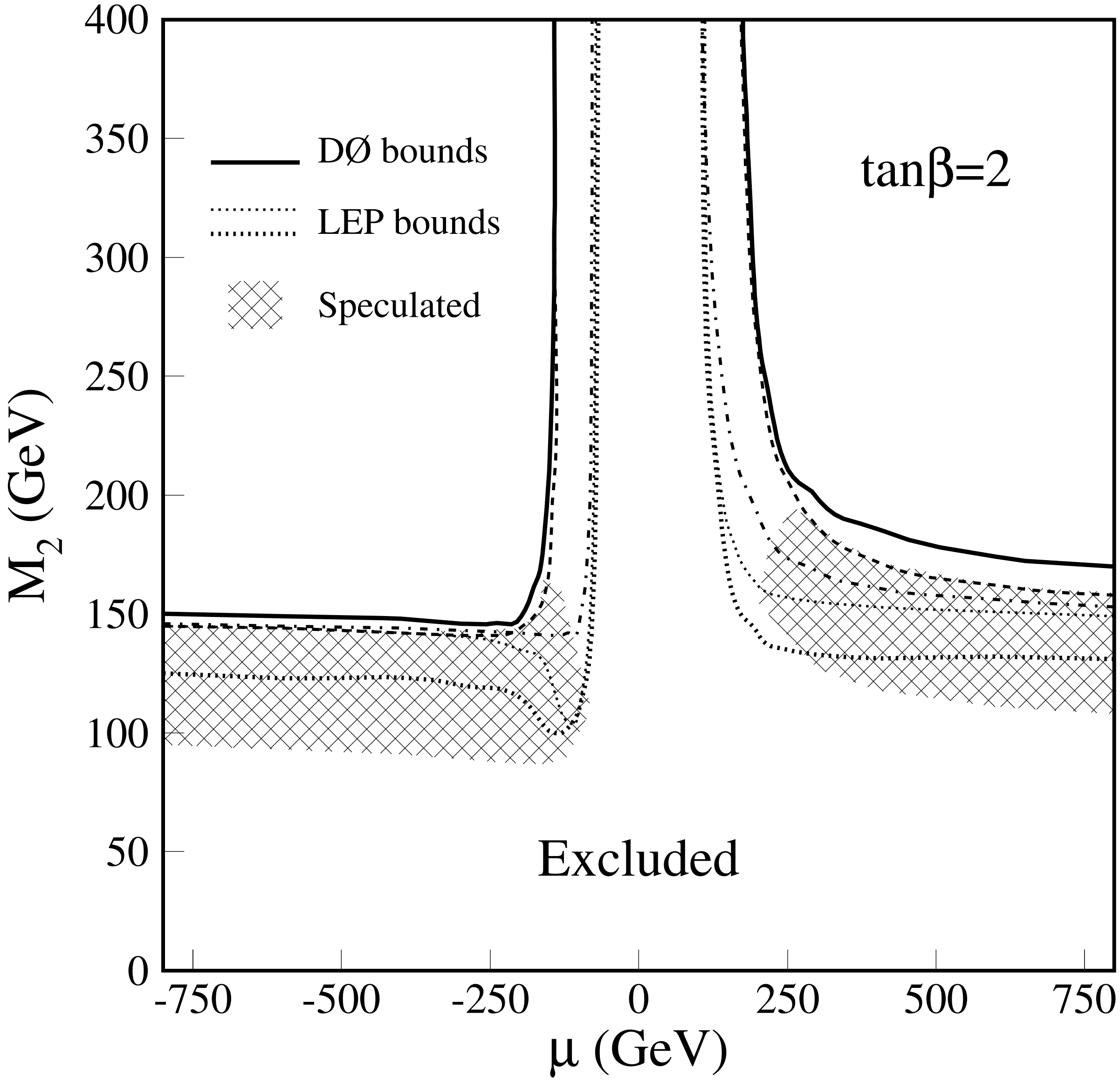

Figure 12: Bounds in the (μ, M_2) plane derived from this analysis for $\tan\beta = 2$. The region below the two solid lines is excluded at 95% CL. Also shown are the bounds estimated in Ref. [3] from the LEP data for $m_{\tilde{e}} = 150$ GeV/c^2 (thick dotted line) and for $m_{\tilde{e}} = 75$ GeV/c^2 (thin dotted line) and the contours of constant $m_{\tilde{\chi}_1^\pm} = 150$ GeV/c^2 (dashed line) and $m_{\tilde{\chi}_1^0} = 75$ GeV/c^2 (dot-dashed line). The hatched areas are speculated in [3] for the chargino interpretation of the CDF event in the model.

The bounds in (μ, M_2) plane for $\tan\beta = 2$ resulted from this analysis are compared with those estimated in Ref. [3] from the LEP data [6] in Fig. 12. The limits from this analysis are stronger than those of the LEP experiments and exclude the region of the parameter space speculated in [3] for the chargino interpretation of the CDF event in the model. Also shown are the mass contours of $m_{\tilde{\chi}_1^\pm} = 150$ GeV/c^2 and $m_{\tilde{\chi}_1^0} = 75$ GeV/c^2. Low mass limits of 150 GeV/c^2 for the lightest chargino and 75 GeV/c^2 for the lightest neutralino are derived from the bounds. The 75 GeV/c^2 lower mass limit on the lightest neutralino also rules out a large part of the parameter space suggested for the scalar electron interpretation [2, 3] of the CDF event in the model. Since the changes in $m_{\tilde{\chi}_1^\pm}$ and $m_{\tilde{\chi}_1^0}$ are primarily responsible for the $\tan\beta$ dependence of the theoretical cross section, the mass limits derived for $\tan\beta = 2$ are also valid for other $\tan\beta$ values studied here ($1 < \tan\beta < 100$). For the same reason, the speculated region of the parameter space for the CDF event is excluded for $1 < \tan\beta < 100$.

4.3 Limits on $\tilde{\chi}_1^\pm\tilde{\chi}_1^\pm$ and $\tilde{\chi}_1^\pm\tilde{\chi}_2^0$ Pair Productions

The pair production of charginos and neutralinos is dominated by the production of $\tilde{\chi}_1^\pm\tilde{\chi}_1^\pm$ and $\tilde{\chi}_1^\pm\tilde{\chi}_2^0$ pairs. Therefore, the null result of the search also constrains the production cross sections of these processes, as often is done for the gravity-mediated models. We note that for a large part of the parameter space ($|\mu| \gg M_2$), the following approximate mass relationship

$$m_{\tilde{\chi}_1^\pm} \approx m_{\tilde{\chi}_2^0} \approx 2 \times m_{\tilde{\chi}_1^0}$$

holds. We therefore express the cross section limits as functions of $m_{\tilde{\chi}_1^\pm}$. These limits are compared with the theoretical cross sections in Fig. 13. The efficiencies and the theoretical cross sections are obtained by varying M_2 while fixing $\tan\beta$ to 2 and μ to -500 GeV. For a given $m_{\tilde{\chi}_1^\pm}$, the efficiency is insensitive to the choice of the parameter values while the theoretical cross section varies within about 10% with the choice of the parameters. The limits are below the theoretical cross sections for a large $\tilde{\chi}_1^\pm$ mass range.

5 Conclusions

We have searched for inclusive high E_T diphoton events with large missing transverse energy using the data collected with the DØ detector during the 1992–1996 Tevatron run at $\sqrt{s}$=1.8 TeV. Such events are predicated in the supersymmetric models with low energy gauge-mediated supersymmetry breaking. No excess of events is found. The null result is interpreted in the minimal supersymmetric standard model with a light gravitino. A large region of the supersymmetry parameter space is excluded. The limits rule out the chargino interpretation of the CDF event and exclude a large part of the parameter space suggested for the scalar electron interpretation in the model.

[6] Most of the supersymmetry cross section at LEP is due to the $t-$channel exchanges of the slepton. Therefore, the LEP limits are strong functions of $m_{\tilde{e}}$. At Tevatron, the charginos and neutralinos are produced primarily through the $s-$channel $W/Z/\gamma$ exchanges.

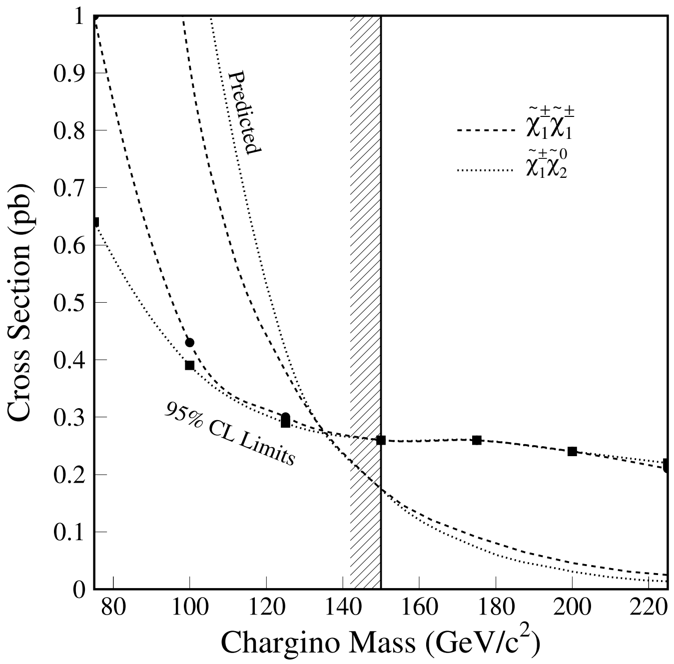

Figure 13: The 95% CL cross section limits and the theoretical cross sections for the $\tilde{\chi}_1^\mp\tilde{\chi}_1^\pm$ and $\tilde{\chi}_1^\mp\tilde{\chi}_2^0$ pair productions as functions of $m_{\tilde{\chi}_1^\pm}$. Also shown is the line representing the mass limit on the lightest chargino derived from this analysis.

6 Acknowledgement

We thank G. Kane for useful discussions and S. Mrenna for his help in using SPYTHIA program.

References

[1] D. Stump, M. Wiest, and C.-P. Yuan, Phys. Rev. **D54** (1996) 1936;
S. Dimopoulos, S. Thomas and J. Wells, Phys. Rev. **D54** (1996) 3283;
K. Babu, C. Kolda, and F. Wilczek, Phys. Rev. Lett. **77** (1996) 3070;
J. Lopez, D. Nanopoulos, and A. Zichichi, Phys. Rev. Lett. **77** (1996) 5168 and hep-ph/9610235;
H. Baer *et al.*, hep-ph/9610358;
J. Bagger *et al.*, hep-ph/9611229;
L. Randall, hep-ph/9612426.

[2] S. Dimopoulos *et al.*, Phys. Rev. Lett. **76** (1996) 3494;
S. Ambrosanio *et al.*, Phys. Rev. Lett. **76** (1996) 3498, Phys. Rev. **D54** (1996) 5395.

[3] J. Ellis, J. Lopez, and D. Nanopoulos, hep-ph/9610470.

[4] P. Fayet, Phys. Lett. **B70** (1977) 461; **B86** (1979) 272; **B175** (1986) 471;
D. Dicus, S. Nandi, and J. Woodside, Phys. Rev. **D41** (1990) 2347 and Phys. Rev. **D43** (1991) 2951.

[5] S. Park, "*Search for New Phenomena in CDF*", 10th Topical Workshop on Proton-Antiproton Collider Physics, edited by R. Raja and J. Yoh, AIP Press, 1995.

[6] DØ Collaboration, S. Abachi *et al.*, "*Search for Diphoton Events with Large Missing Transverse Energy in $p\bar{p}$ Collisions at $\sqrt{s}$=1.8 TeV*", hep-ex/9612011 and Fermilab-Pub-96/446-E.

[7] S. Mrenna, "*SPYTHIA, A Supersymmetric Extension of PYTHIA 5.7*", hep-ph/9609360.

[8] H.U. Bengtsson and T. Sjöstrand, Comp. Phys. Comm. **46** (1987) 43;
T. Sjöstrand, Comp. Phys. Comm. **82** (1994) 74.

[9] H. L. Lai *et al.*, Phys. Rev. **D51** (1995) 4763.

[10] M. Carena *et al.*, Nucl. Phys. **B369** (1992) 33;
J. Bagger *et al.*, Phys. Rev. Lett. **55** (1985) 920.

[11] DØ Collaboration, S. Abachi *et al.*, Nucl. Instrum. Methods **A338** (1994) 185.

[12] R. Brun and F. Carminati, CERN Program Library Long Writeup W5013, 1993 (Unpublished).

[13] S. Chopra, U. Heintz and M. Narain, "*Comparison of Electron ID Efficiencies in Run 1A and 1B*", DØnote 2351.

[14] M. Kelly, "*Test of the Standard Model of Electroweak Interactions by Measuring the Anomalous $WW\gamma$ couplings at $\sqrt{s}$=1.8 TeV*", Ph.D. Thesis, Univ. of Notre Dame (1996) (Unpublished);
DØ Collaboration, S. Abachi *et al.*, "*Limits on Anomalous $WW\gamma$ Couplings from $p\bar{p} \to W\gamma + X$ Events at $\sqrt{s}$=1.8 TeV*", hep-ex/9612002 and Fermilab-Pub-96/434-E.

[15] G. Landsberg, "HITSINFO *package*", to be released as a DØnote.

[16] G. Landsberg, "*Search for Anomalous Couplings in the $Z(\nu\nu)\gamma$ Channel with Run Ia Data*", DØnote #3047.

[17] H. Greenlee, M. Narain, P. Singh, "*The Search for a Fourth Generation Quark (b') using Flavor-Changing Neutral Current Decay Signatures*", DØnote xxx.
DØ Collaboration, S. Abachi *et al.*, "*Search for a Fourth Generation Charge $-1/3$ Quark via Flavor Changing Neutral Current Decay*", hep-ex/9611021 and Fermilab-Pub-96/430-E.

[18] Particle Data Group, R. M. Barnett *et al.*, Phys. Rev. **D54**, (1996) 165;
J. Hobbs, the limit program http://d0sgi0.fnal.gov/~hobbs/limit_calc.html;
I. Bertram *et al.*, "*A Recipe for the Construction of Confidence Limits*", DØnote #2775A.

Appendix: Comparisons with an Earlier Analysis

In this section, the analysis described in this note is compared with that reported in Ref. [6]. Table 5 summarizes the efficiencies of the two analyses for the models studied in [6]. For almost all the cases, a factor of two or more increase in efficiency is obtained. The higher efficiency is a direct benefit of the improved electron rejection of the photon identification. The HITSINFO selection of the photon identification reduced the $e\gamma\not\!\!E_T$ background to a negligible level and therefore rendered event topology based selection employed in Ref. [6] designed to reduce $e\gamma\not\!\!E_T$ background unnecessary. Consequently, the efficiency for supersymmetry is dramatically increased.

Process	Mass (GeV/c^2)			Ref. [6]		This Analysis	
	$\tilde{\ell}$	$\tilde{\chi}_2^0$	$\tilde{\chi}_1^0$	ϵ	σ (pb)	ϵ	σ (pb)
$\tilde{e}\tilde{e}$	100	80	30	–	–	0.157 ± 0.012	0.31
	100	80	40	–	–	0.140 ± 0.011	0.35
	100	80	50	–	–	0.113 ± 0.010	0.43
	100	90	50	0.048 ± 0.007	0.715	0.134 ± 0.011	0.36
	100	90	60	–	–	0.108 ± 0.010	0.45
	100	90	70	–	–	0.061 ± 0.008	0.82
$\tilde{\nu}\tilde{\nu}$	70	50	30	0.036 ± 0.006	0.995	0.056 ± 0.007	0.88
	70	60	30	0.044 ± 0.007	0.805	0.092 ± 0.009	0.54
	70	60	50	0.001 ± 0.001	–	0.008 ± 0.003	22
	80	65	55	0.007 ± 0.002	21.6	0.014 ± 0.004	4.8
	80	70	60	0.005 ± 0.002	20.8	0.014 ± 0.004	5.0
	90	70	65	–	–	–	–
	90	80	65	0.018 ± 0.004	2.13	0.035 ± 0.006	1.48
	90	80	70	0.004 ± 0.002	54.7	0.014 ± 0.004	5.0
	100	90	70	0.046 ± 0.007	0.765	0.068 ± 0.008	0.73
	100	90	80	0.010 ± 0.003	4.65	0.008 ± 0.003	17
$\tilde{\chi}_2^0\tilde{\chi}_2^0$		60	30	0.049 ± 0.007	0.688	0.106 ± 0.010	0.47
		60	40	0.038 ± 0.006	0.935	0.069 ± 0.008	0.72
		70	30	0.063 ± 0.008	0.555	0.142 ± 0.011	0.34
		70	40	0.052 ± 0.007	0.680	0.115 ± 0.010	0.42
		70	50	0.035 ± 0.006	1.03	0.072 ± 0.008	0.68
		80	30	0.072 ± 0.009	0.471	0.162 ± 0.012	0.30
		80	40	0.056 ± 0.008	0.610	0.146 ± 0.011	0.33

Table 5: Efficiencies (ϵ) and 95% CL cross section limit for the $\gamma\gamma\not\!\!E_T$ events of the selection reported in this note and of that reported in [6]. The Monte Carlo events are courtesy of J. Womersley.

For these Monte Carlo events, $\tilde{\chi}_2^0$ is assumed to decay into $\gamma + \tilde{\chi}_1^0$ with a 100% branching ratio. Consequently, the photon E_T and $\not\!\!E_T$ are largely determined by the mass difference between $\tilde{\chi}_2^0$ and $\tilde{\chi}_1^0$. Therefore, the efficiency is a strong function of $m_{\tilde{\chi}_2^0} - m_{\tilde{\chi}_1^0}$ and depends on the process weakly as shown in Fig. 14 for the three processes. For the same reason, the 95%

CL total cross section limit is displayed in Fig. 15.

Table 6 shows the efficiency breakdowns of this analysis and the 95% C.L. detectable cross section limits (σ_D) of diphoton events passing the kinematic requirements on photons and $\not\!\!E_T$ for three different processes. The cross section limits are somewhat process-dependent. For $m_{\tilde{\chi}_2^0} - m_{\tilde{\chi}_1^0} \geq 30$ GeV/c^2, the limit on the detectable cross section is generally less than 0.19 pb, almost independent of the processes.

Process	Mass (GeV/c^2)			Efficiency					σ_D (pb)
	$\tilde{\ell}$	$\tilde{\chi}_2^0$	$\tilde{\chi}_1^0$	ϵ_K	ϵ_R	ϵ_{ID}	ϵ	$\epsilon_D (= \epsilon/\epsilon_K)$	95% CL
$\tilde{e}\tilde{e}$	100	80	30	0.545	0.683	0.424	0.157	0.288 ± 0.026	0.17
	100	80	40	0.504	0.653	0.426	0.140	0.277 ± 0.026	0.18
	100	80	50	0.424	0.630	0.424	0.113	0.267 ± 0.027	0.18
	100	90	50	0.526	0.603	0.424	0.134	0.255 ± 0.024	0.19
	100	90	60	0.425	0.609	0.421	0.108	0.255 ± 0.026	0.19
	100	90	70	0.285	0.505	0.424	0.061	0.215 ± 0.029	0.23
$\tilde{\nu}\tilde{\nu}$	70	50	30	0.193	0.710	0.414	0.056	0.292 ± 0.040	0.17
	70	60	30	0.324	0.679	0.418	0.092	0.283 ± 0.031	0.17
	70	60	50	0.052	0.365	0.414	0.008	0.151 ± 0.054	1.2
	80	65	55	0.074	0.446	0.424	0.014	0.189 ± 0.051	0.35
	80	70	60	0.067	0.478	0.429	0.014	0.205 ± 0.056	0.33
	90	70	65	0.008	–	–	–	–	–
	90	80	65	0.155	0.542	0.421	0.035	0.225 ± 0.039	0.23
	90	80	70	0.073	0.438	0.425	0.014	0.186 ± 0.051	0.34
	100	90	70	0.275	0.589	0.419	0.068	0.256 ± 0.031	0.20
	100	90	80	0.069	0.304	0.420	0.009	0.122 ± 0.042	1.2
$\tilde{\chi}_2^0\tilde{\chi}_2^0$		60	30	0.359	0.713	0.413	0.106	0.294 ± 0.031	0.17
		60	40	0.243	0.683	0.415	0.069	0.283 ± 0.036	0.18
		70	30	0.455	0.749	0.417	0.142	0.313 ± 0.029	0.16
		70	40	0.394	0.706	0.416	0.115	0.293 ± 0.029	0.17
		70	50	0.270	0.644	0.416	0.072	0.268 ± 0.033	0.18
		80	30	0.527	0.734	0.420	0.162	0.307 ± 0.027	0.16
		80	40	0.479	0.729	0.418	0.146	0.305 ± 0.028	0.16

Table 6: Breakdowns of efficiencies and the 95% CL detectable cross section limits for diphoton events passing the kinematic requirements discussed in this note. The error on ϵ_D includes both statistical and systematic errors.

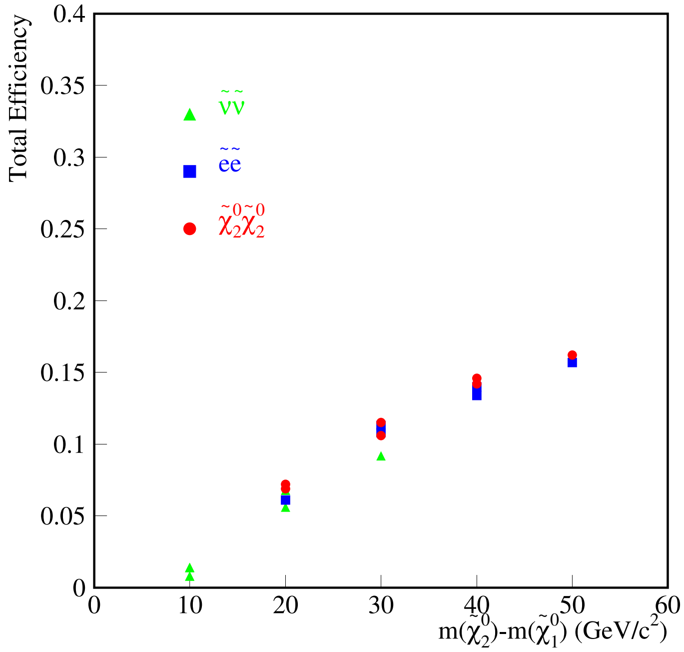

Figure 14: The total efficiency as a function of $m_{\tilde{\chi}_2^0} - m_{\tilde{\chi}_1^0}$ for $\tilde{\nu}\tilde{\nu}$, $\tilde{e}\tilde{e}$ and $\tilde{\chi}_2^0\tilde{\chi}_2^0$ events.

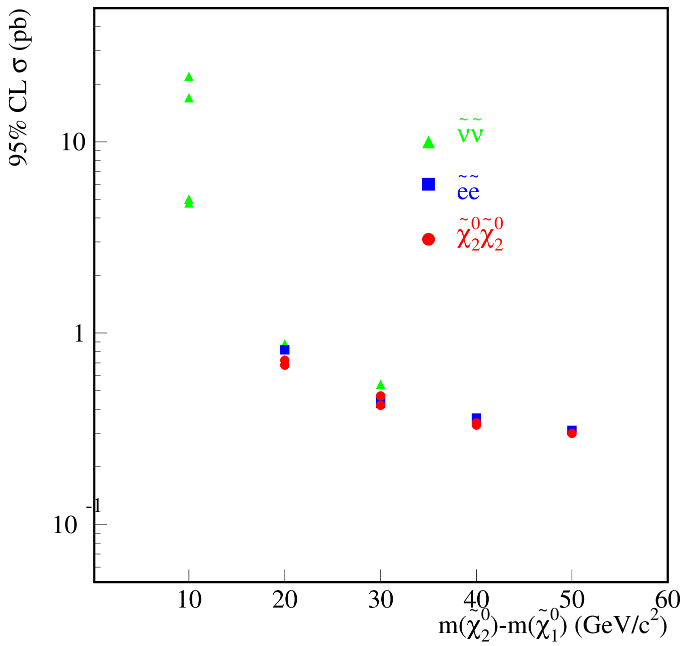

Figure 15: The 95% cross section limit as a function of $m_{\tilde{\chi}_2^0} - m_{\tilde{\chi}_1^0}$ for $\tilde{\nu}\tilde{\nu}$, $\tilde{e}\tilde{e}$ and $\tilde{\chi}_2^0\tilde{\chi}_2^0$ events.